Springer Verlag Book Chapter in
"Fractals and Disordered Systems" Vol II
Eds. A. Bunde and S. Havlin

4 Kinetics and Spatial Organization of Competitive Reactions

S. Redner and F. Leyvraz

4.1 Introduction

In this article, we review some kinetic and geometric properties of two-species annihilation in which an encounter between two distinct species A and B leads to the formation of an inert product I, $A + B \rightarrow I$ [4.1]. Examples of this reaction include electron-hole recombination in irradiated semiconductors [4.2], catalytic reactions on surfaces [4.3], exciton dynamics [4.4], and annihilation of primordial monopoles in the early universe [4.5]. At a more abstract level, two-species annihilation is a realization of an interacting Brownian particle system, a connection which has been helpful in establishing rigorous results [4.6].

Under homogeneous symmetric conditions, *i. e.*, where the two species are initially present at equal, spatially uniform concentrations, or are fed into the system homogeneously at equal rates, there is a spontaneous symmetry breaking in which large-scale single species heterogeneities form [4.7-18]. This spatial organization invalidates the mean-field approximation and its corresponding predictions. One of our goals is to outline mechanisms that lead to this spatial organization in two-species annihilation. In addition to the microscopic reaction itself, the rate of transport (usually diffusion) and the rate of input of new reactants play a fundamental role in governing the reaction kinetics. We shall discuss how the interplay between external input, the microscopic reaction, and transport influence the overall reaction kinetics and the growth of spatial heterogeneities.

Fig. 4.0. Position of A and B particles in two species annihilation on a square 1000×1000 lattice after 1000 time steps. Here one of the species is static. To make each individual particle visible, 9 colored pixels are used to mark the particle position. Notice the clearly defined domains in which the mobile species are smoothly distributed while the immobile species have a singular spatial distribution. Since the immobile species are strongly clustered, the display algorithm distorts their apparent concentration (Figure courtesy of Stephen Harrington).

To analyze two-species annihilation, a crucial observation is that the difference in the concentration of A's and B's is conserved, both globally, as well as in each individual reaction. Thus the dynamical equations which describe the densities of A's and B's contain the same reaction term. Therefore the equation for the concentration difference is a linear one in which only transport and input terms appear. This observation, together with plausible physical hypotheses about the system, provide a solution for the individual species concentrations.

When there is no input or back reaction, the reactant densities decay monotonically. If the microscopic reaction rate is small compared to the rate of collisions between reactants, the process is *reaction-limited.* In this case, many collisions occur before a reaction event so that there is time for substantial mixing. Thus one expects the mean-field predictions to hold. In the opposite *diffusion-limited* process, the microscopic reaction is fast and the overall process is limited by the rate at which reactive pairs are brought together. In low spatial dimension, this implies lack of mixing, a feature which is responsible for large-scale coarsening of the reactant distributions. To quantify the distinction between these two limiting situations, consider the relation between the two fundamental time scales t_R, the typical time for a given particle to react with an arbitrary particle, and t_D, the time required for a particle to diffuse to a nearest neighbor. If the reactant concentration is $c(t)$, then within mean-field theory t_R is of the order of $1/(kc)$, where k is the rate constant, whereas for diffusing reactants t_D is of the order of $c^{-2/d}/D$, where d is the spatial dimension. Thus for $d \leq 2$, the system eventually reaches the limiting situation where $t_R \ll t_D$, *i. e.*, the diffusion-limited case. If $k \ll 1$, however, there may be a large crossover regime before diffusion-limited behavior is reached [4.11]. In fact, for two-species annihilation, the asymptotic diffusion-limited regime extends up to $d = 4$ since domain formation greatly increases t_D relative to a homogeneous system.

When the reactants are externally fed into the system at equal rates, the balance between the input and annihilation may lead to a steady state [4.15-18]. However, diffusive fluctuations can still promote a continuously coarsening pattern of A-rich and B-rich domains and steady behavior occurs only when the input is sufficiently coupled in both time and space to counteract diffusive fluctuations [4.16]. An important limiting case arises when the reactants are static after input. This can be viewed as a model catalytic reaction in which the input corresponds to the adsorption of reactants onto vacant sites of a catalytic surface (whose dimension need not be two). The adsorbates remain immobile, a characteristic feature of the adsorption of many gases on metal surfaces. A nearest-neighbor adsorbed AB pair forms a product at some finite rate which then immediately desorbs. These steps define the *monomer-monomer* catalysis model [4.19-22], in which the formation of the AB product is assisted by the mere presence of the catalytic surface. Even when the adsorption rates of the two species are equal, this deposition of static particles leads to growing domains of A and B form due to fluctuation in the reactant input [4.19-21]. This coarsening terminates in *saturation*, where a finite-size surface is fully occupied by only one of the two species, and further reactions cannot occur [4.22].

The tendency for domain formation in two-species annihilation confines the microscopic reaction to the interfacial regions between domains. This motivates the investigation of the reaction under heterogeneous conditions which promote the existence of a localized interface [4.23-35]. Two such examples include a system with initial semi-infinite domains of A's and B's which meet at a common boundary, or a finite system with input of A's and B's at opposite edges. Such geometries may also be more amenable to experimental realizations than a homogeneous system [4.27]. For these situations, the investigation of the reactive interface opens a rich variety of phenomena from which useful insights about the microscopic reaction process can be obtained.

Our goal is to elucidate kinetic and spatial organization effects in these situations. We first discuss irreversible two-species annihilation for spatially homogeneous systems in Sect. 4.2. For equal initial densities of the two species, some basic geometric properties of the mosaic of continuously growing A- and B-domains are outlined. Although domains grow diffusively, a multiplicity of independent length scales are needed to characterize the spatial distribution of reactants properly [4.36,37]. In Sect. 4.3, we discuss the kinetics of the reaction under steady, spatially homogeneous input, where an exact solution for the continuum system can be derived [4.16-18]. For the special case of no transport (monomer-monomer model) and infinitely large input rate, the lattice system can be mapped onto a kinetic Ising model [4.38], a birth-death process (in one dimension only) [4.39], and the "voter" model [4.40]. Through these mappings, the exact solution for the kinetics and the spatial correlations can be found. These results account for the coarsening of domains and the ultimate saturation of the surface by a single species. In Sect. 4.4, we discuss the reaction kinetics of the spatially inhomogeneous system [4.23-35]. Dimensional arguments of a mean-field spirit are used to characterize the geometry of the "reactive zone" at the interface. This approach is inadequate in low spatial dimensions, however, and we discuss analytical approaches and numerical investigations of interfacial profiles in one dimension. We give a brief summary in Sect. 4.5.

4.2 Irreversible Homogeneous Reaction

4.2.1 Decay of the Density

Consider two diffusing species A and B which are originally distributed at random with respective concentrations $c_A(0)$ and $c_B(0)$. When two opposite species particles approach within the (fixed) reaction radius, they react irreversibly to form a third, inert species, which is then disregarded. For unequal initial concentrations, the minority concentration quickly decays to zero, whereas the majority concentration approaches a constant. For equal initial densities, the concentration of each species, $c(t)$, decays as a power-law in time. Associated

with this relatively slow kinetics is a large-scale spatial organization of reactants in low spatial dimensions. These features are the focus of this section.

To estimate the decay of the density within a mean-field approximation, note that in a time interval of order $1/c$, each particle will come in contact with another particle, on average. Consequently, in a time interval $\Delta t \propto 1/kc$, where k is the reaction rate, the concentration will decrease by an amount of order c, that is, $\Delta c \propto -c$. This gives the mean-field rate equation

$$\dot{c} \cong \frac{\Delta c}{\Delta t} \propto -kc^2, \tag{4.1}$$

with solution $c(t) = c(0)/(1 + kc(0)t) \sim (kt)^{-1}$. Thus the exponent of the decay is -1, and the time scale is set by k. This exponent value turns out to be correct only for spatial dimension $d \geq 4$, corresponding to the regime of validity of the mean-field prediction. However, this prediction for the exponent is clearly incorrect for spatial dimension $d < 2$ because the time interval for reactions to occur is now $\Delta t \propto \ell^2/D$, where $\ell \propto c^{-1/d}$ is the typical interparticle spacing and D is the diffusion coefficient. Notice that the reaction rate does not enter into this time scale because random walk trajectories are compact. Thus if two reactants collide once, they will collide an infinite number of times and the reaction rate rescales to a large value. The rate equation now becomes,

$$\dot{c} \cong \frac{\Delta c}{\Delta t} \propto Dc^{1+2/d}, \tag{4.2}$$

with solution $c(t) \sim (Dt)^{-d/2}$. This approach shows how microscopic details determine the effective "order" of the reaction.

Both of the above predictions for $c(t)$ are incorrect for $d \leq 4$ because domains containing only one of the two species form [4.10-14,37]. This invalidates the homogeneity assumption of the mean-field approximation. Explicit account of the local density fluctuations are needed to understand the long-time behavior of $c(t)$. Within a scaling formulation, this can be accomplished by considering a system with slightly different initial densities [4.11]. For this system, there exist regions of characteristic size $\xi \propto (\delta c)^{-2/d}$, where δc is the initial density difference, below which the identity of the local majority species is ambiguous because of local density fluctuations. Consequently, for times less than a characteristic time scale $t_\xi \sim \xi^2/D$, the density decays as a power law, while a faster than power law decay is expected at longer times. Since this time scale is simply related to the conserved density difference, it is possible to infer the form of the decay through scaling ideas.

An explicit, but qualitative version of the above approach is to note that the number difference between A's and B's in a finite volume Ω of linear dimension $\mathcal{L}$ remains nearly constant during the time for a particle to traverse the volume by diffusion, $t_{\mathcal{L}} \sim \mathcal{L}^2/D$. However, at $t = 0$, this difference is of the order to the square root of the initial particle number,

$$N_A - N_B \approx \pm\sqrt{c(0)}\mathcal{L}^{d/2}. \tag{4.3}$$

If we assume that A's are initially the local majority in Ω, then for $d \leq 4$, essentially no B's will remain at time $t_{\mathcal{L}}$. Thus $N_A(t_{\mathcal{L}})$ is approximately equal to $\sqrt{c(0)}\mathcal{L}^{d/2}$. Elimination of $\mathcal{L}$ in favor of t gives,

$$c(t) \approx N(t)/\mathcal{L}^d \sim \sqrt{c(0)}\,(Dt)^{-d/4}, \qquad (d \leq 4). \tag{4.4}$$

Thus a homogeneous system is predicted to evolve into a mosaic of domains whose individual identities are determined by the species in the local majority in the initial state. At time t, these domains will be of typical length $\sqrt{Dt}$ within which a single species of density $\sqrt{c(0)}(Dt)^{-d/4}$ remains.

The above line of reasoning is invalid for $d > 4$, however. To appreciate what occurs in this case, suppose that a reaction-generated domain mosaic is used as an initial condition. For domains of linear dimension $\mathcal{L}$ and local concentration of order $\mathcal{L}^{-d/2}$, let us estimate the probability that an A particle is unsuccessful in crossing a typical B domain. For $d > 4$, the particle needs $\mathcal{L}^2$ time steps to cross and will visit $\mathcal{L}^2$ distinct B-occupied sites during the traversal. At each site, the A will react with a probability that is of the order of the B concentration, $\mathcal{L}^{-d/2}$. Therefore the probability that an A particle is unsuccessful in traversing a B domain is of the order of $\mathcal{L}^{(4-d)/2}$. Since this vanishes as $\mathcal{L} \to \infty$ if $d > 4$, the domain mosaic is unstable to diffusion for $d > 4$.

A more rigorous argument for the fluctuation-dominated behavior focuses on the evolution of the local concentration difference $c_-(\boldsymbol{x},t) \equiv c_A(\boldsymbol{x},t) - c_B(\boldsymbol{x},t)$. This difference evolves by pure diffusion [4.10], so that the time dependence of the Fourier transform is simply $c_-(\boldsymbol{k},t) = c_-(\boldsymbol{k},t=0)e^{-Dk^2t}$. At long times, the existence of domains implies that there is minimal coexistence of A's and B's. Thus the product $c_A(\boldsymbol{x},t)c_B(\boldsymbol{x},t) = 0$, which implies that

$$\begin{aligned}\int d\boldsymbol{x}\, c_A(\boldsymbol{x},t)^2 &\sim \frac{1}{2}\int d\boldsymbol{k}\, |c_-(\boldsymbol{k},0)|^2 \exp(-Dk^2t) \\ &\propto (Dt)^{-d/2}\int d\boldsymbol{q}\, |c_-(\boldsymbol{q}/(Dt)^{1/2},t)|^2 \exp(-q^2).\end{aligned} \tag{4.5}$$

For a random initial condition, $|c_-(\boldsymbol{k},t=0)|^2 = N$ for all $\boldsymbol{k}$, since the mean-square involves the sum of N random unit vectors. Thus the integral over $\boldsymbol{q}$ in Eq. (4.5) is independent of t, so that $\langle c_A(\boldsymbol{x},t)^2\rangle \sim \frac{N}{V}\,(Dt)^{-d/2}$. Finally the assumption of no cross correlations implies that $\langle c_A(\boldsymbol{x},t)^2\rangle \cong \langle c_A(\boldsymbol{x},t)\rangle^2$ and Eq. (4.4) is reproduced. Notice that the random initial condition is a crucial aspect for obtaining the anomalous slow decay. In particular, for correlated initial conditions with no long-wavelength fluctuations in $c_-(\boldsymbol{x},t)$, the integral over $\boldsymbol{q}$ will vanish as $t \to \infty$, thus invalidating the above reasoning [4.12,41].

It is also instructive to give a dimensional argument for the $\sqrt{c(0)}$ prefactor in the expression Eq. (4.4) for the density. There are only two dimensionless parameters that can be constructed using the available model parameters D, k and $c(0)$, namely

$$\tau = Dc(0)^{2/d}t, \qquad x = \frac{Dc(0)^{(2-d)/d}}{k}. \tag{4.6}$$

Thus on purely dimensional grounds, $c(t)$ must be equal to $c(0)\Phi(x,\tau)$ for arbitrary x and τ. If $c(t) \propto t^{-d/4}$ as $t \to \infty$, then $\Phi(x,\tau)$ must have the form $C(x)\tau^{-d/4}$ as $\tau \to \infty$. This reproduces Eq. (4.4), except for a possible prefactor which depends on x. If one further assumes that the asymptotic behavior of the concentration is independent of k, one obtains exactly Eq. (4.4). The numerical verification of the $\sqrt{c(0)}$ prefactor is not fully settled, however. While it is reasonably confirmed in one dimension [4.11], Cornell *et al.* appear to find a different initial density dependence in their two-dimensional simulations [4.42]. Further work is needed to clarify the origin of this discrepancy.

By further assuming that the limit $k \to 0$ corresponds to the mean-field behavior, one obtains $\Phi(x,\tau) \approx x/\tau$, as $x \to \infty$. This indicates that the crossover from mean-field to diffusion-limited behavior occurs when $\tau \approx x^{4/(4-d)}$. Thus if $k \ll 1$, there is a large temporal domain of mean-field behavior [4.11]. This is physically reasonable, since the low reaction probability renders small-scale heterogeneities transparent. For long times, however, sufficiently large heterogeneities occur which are opaque to the local minority species. Thus the fluctuation-dominated behavior of Eq. (4.4) should result in sufficiently low spatial dimension.

The fluctuation-controlled kinetics is not qualitatively modified by varying the diffusion constants of the two species, even in the extreme case where one species is immobile. The basic analysis about fluctuations can also be generalized to fractals [4.43-45,37], where one obtains that $c(t_{\mathcal{L}})$ is approximately given by $\sqrt{c(0)}\mathcal{L}^{-d_f/2}$, and $t_{\mathcal{L}}$ is equal to $\mathcal{L}^{d_w}$, leading to the time dependence, $c(t) \sim t^{-d_s/4}$. Here, d_f is the fractal dimension, d_w is the dimension of a random walk on the fractal, and d_s the spectral dimension. While an alternative line of reasoning has recently been given [4.44], numerical results do appear to suggest that the decay kinetics is determined by simply making the replacement $d \to d_s$ [4.45].

Thus the kinetics of the $A + B \to I$ reaction is determined by the competition between A- and B-domains. This process depends fundamentally on geometric features of these domains, such as the interparticle distances between closest-neighbor like and unlike species and the domain size distribution. Some unexpected properties emerge from these quantities as we discuss in the rest of this section.

4.2.2 Interparticle Distances

A surprising feature of the spatial distribution of reactants is that the typical distances between AA and AB closest-neighbor pairs, ℓ_{AA} and ℓ_{AB}, respectively, grow with different powers of t for $d < 3$ [4.37]. This indicates that there is a non-trivial modulation in the reactant density over the extent of a domain. To determine the time evolution of ℓ_{AB} in one dimension, consider the behavior of c_{AB}, the concentration of closest-neighbor AB pairs. In a time increment $\Delta t \sim \ell_{AB}^2/D$, there is sufficient time for essentially all such AB pairs to react, since one-dimensional random walks are compact. Consequently, the

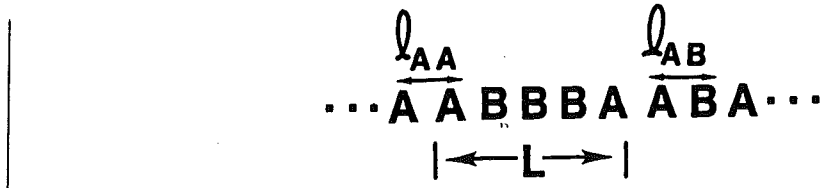

Fig. 4.1. Definition of fundamental interparticle distances in one dimension: the typical distance between closest-neighbor same species particles, ℓ_{AA}, the distance between closest-neighbor unlike species, ℓ_{AB}, (the gap between domains), and the typical domain length, L.

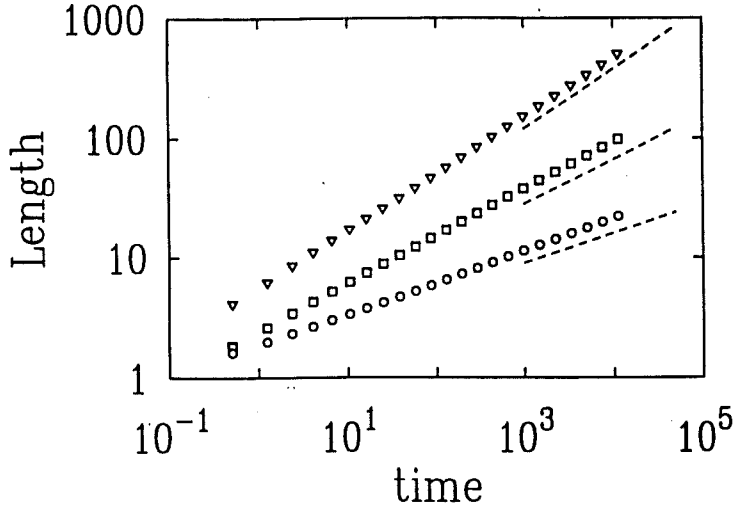

Fig. 4.2. Time dependence of $\langle \ell_{AA} \rangle$ (○), $\langle \ell_{AB} \rangle$ (□), and the average domain length, $\langle L \rangle$, (▽) for a one-dimensional system when both species have the same mobility. The dashed lines of respective slopes of 1/4, 3/8, and 1/2 serve as guides to the eye.

number of reactions per unit length is of the order of c_{AB}. Thus the rate of change of the concentration is

$$\frac{\Delta c}{\Delta t} \approx -k \frac{c_{AB}}{\ell_{AB}^2/D}. \tag{4.7}$$

This relation holds only for spatial dimension $d < 2$, since the compactness of random walks is an essential hypothesis. Since we independently know the left-hand side of Eq. (4.7) from $c(t)$ itself, the behavior of c_{AB} determines the time dependence of ℓ_{AB}. In one dimension, c_{AB} scales as $(Dt)^{-1/2}$, since the typical domain size is $(Dt)^{1/2}$ and there is one AB pair per domain. Therefore [4.37]

$$\ell_{AB} \sim c(0)^{-1/4} (Dt)^{3/8}. \tag{4.8}$$

Thus at least three lengths are needed to characterize the spatial distribution of reactants: the average domain size, which scales as $(Dt)^{1/2}$; the typical interparticle spacing, which scales as $c(t)^{-1} \propto t^{1/4}$; and the interdomain gap ℓ_{AB}. The stronger time dependence of ℓ_{AB} compared to that of the typical interparticle spacing is a manifestation of an effective "repulsion" between opposite species particles. Nearby opposite species pairs annihilate preferentially, leaving behind a population where opposite species are separated by a distance which is larger than the typical interparticle separation.

The time dependence of the *average* distance between same species nearest-neighbor pairs, $\langle \ell_{AA} \rangle$, is characterized by an exponent which is close to, but measurably larger than the value of 1/4 that one might naively expect. This larger exponent value arises because the local density vanishes near the domain edge and causes the average distance between neighboring particles to be larger than the typical distance. Below, we show that this modulation in the domain profile leads to a multiplicative logarithmic factor in the scaling behavior of $\langle \ell_{AA} \rangle$ compared to the typical value.

Remarkably, the average interparticle distances depend on the mobility ratio of both species. The most interesting situation is that of one immobile species (B), where the effective exponent for $\langle \ell_{BB} \rangle$ slowly approaches its asymptotic value, whereas the effective exponent for $\langle \ell_{AA} \rangle$ is roughly the same as in the equal mobility case. Interestingly the effective exponent for $\langle \ell_{BB} \rangle$ remains *below* 1/4 over a large temporal range, even though the asymptotic value of this exponent can be bounded from below by 1/4. This anomaly stems from a short-distance power-law tail in the distribution of separations between neighboring B's, a feature which is a vestige of the initial distribution of BB separations.

To generalize to spatial dimension $1 \leq d \leq 2$, note that the time dependence of ℓ_{AB} should still follow by applying Eq. (4.7), since it holds whenever random walks are compact. To estimate c_{AB}, we assume a smooth domain perimeter of length $t^{(d-1)/2}$ and that particles in the perimeter zone are separated by a distance of the order of ℓ_{AB}, irrespective of identity. This approach leads to the following generalization of Eq. (4.8),

$$\ell_{AB} \propto t^{\frac{(d+2)}{4(d+1)}}, \qquad c_{AB}(t) \propto t^{-\frac{d(d+3)}{4(d+1)}}, \tag{4.9}$$

which yields $\ell_{AB} \sim t^{1/3}$ and $c_{AB}(t) \sim t^{-5/6}$ in $d = 2$.

In three and higher dimensions, the transience of random walks implies that two neighboring opposite species particles which are confined to a region of linear dimension ℓ_{AB} will react within a time of the order of ℓ_{AB}^d (rather than ℓ_{AB}^2). Consequently, Eq. (4.7) must be modified to

$$\frac{\Delta c}{\Delta t} \approx -k \frac{c_{AB}}{\ell_{AB}^d}. \tag{4.10}$$

This relation, together with the assumption of a smooth interfacial region between domains, gives, in d dimensions:

$$c_{AB} \approx t^{-\frac{d^2+5d-4}{4(2d-1)}}, \qquad \ell_{AB} \approx t^{\frac{d+2}{4(2d-1)}}, \tag{4.11}$$

which coincides with Eq. (4.9) at $d = 2$. For $d = 3$ Eq. (4.11) yields

$$c_{AB} \approx t^{-1}, \qquad \ell_{AB} \approx t^{1/4}. \tag{4.12}$$

These exponents represent limiting values: Indeed, there is no mechanism whereby $\langle \ell_{AB} \rangle$ could become less than $\langle \ell_{AA} \rangle$, and the non-trivial scaling of interparticle distances disappears in three dimensions and above. This has been confirmed in large-scale three-dimensional numerical simulations [4.46]. Thus

for $d \geq 3$, there is no appreciable depletion in the average density in the interfacial region between domains. Thus the predictions of Eq. (4.11) are expected to be valid only below an upper critical dimension which is equal to 3. The existence of this critical dimension for the behavior of the interparticle distances is remarkable, as the upper critical dimension equals 4 for the behavior of $c(t)$, and equals 2 for the case of two-species annihilation with input or back reactions.

4.2.3 Domain Size Distribution in One Dimension

A more complete understanding of the spatial organization of reactants can be gained by considering the distribution of domain sizes. This distribution can be deduced indirectly by considering the dynamics of the domain walls (W), roughly defined as the midpoint between two unlike neighboring particles. Since individual particles diffuse, it is natural to postulate that the walls also move diffusively. This approximation is questionable, however, as annihilation events can lead to large distance jumps in the wall position. Nevertheless, we adopt the hypothesis of diffusing domain walls as it leads to several correct predictions about the domain size distribution. Since domain walls annihilate on contact, their dynamics should coincide with that of the density in the exactly-soluble single species annihilation model, $W + W \to I$ [4.47-50]. Thus the distribution of domain sizes in two-species annihilation corresponds to the interparticle distance distribution in single-species annihilation. This latter quantity is known to decay exponentially for large separations and vary linearly in separation in the small distance limit [4.47].

Consequently the number of domains of length L at time t, $N(L,t)$, may be written in the scaling form

$$N(L,t) \sim \frac{1}{t}\Phi(L/\sqrt{t}) \tag{4.13}$$

where the scaling function $\Phi(x)$ has the following asymptotic limits,

$$\begin{aligned} \Phi(x) &\sim x \qquad && x \to 0 \\ &\sim e^{-Cx}, && x \to \infty. \end{aligned} \tag{4.14}$$

The prefactor $1/t$ in Eq. (4.13) ensures that the system length, $\sum LN(L,t)$, is time independent. This scaling form has several non-trivial consequences which have been verified numerically. For example, the small-x behavior of $\Phi(x)$, leads to a $t^{-3/2}$ decay of the number of fixed-size domains.

When the B's are immobile, the domain size distribution develops an $x^{-1/2}$ power law tail in the small-size limit. This exponent value can be accounted for by the following random walk argument: Consider the initial density difference $c_-(x,0) = c_A(x,0) - c_B(x,0)$ which traces a random walk along x. As a function of time, this function relaxes by diffusion in the regions where the density difference is positive, while only the reactions influence the evolution of regions of negative density difference. Thus any region where $c_-(x,0)$ was initially

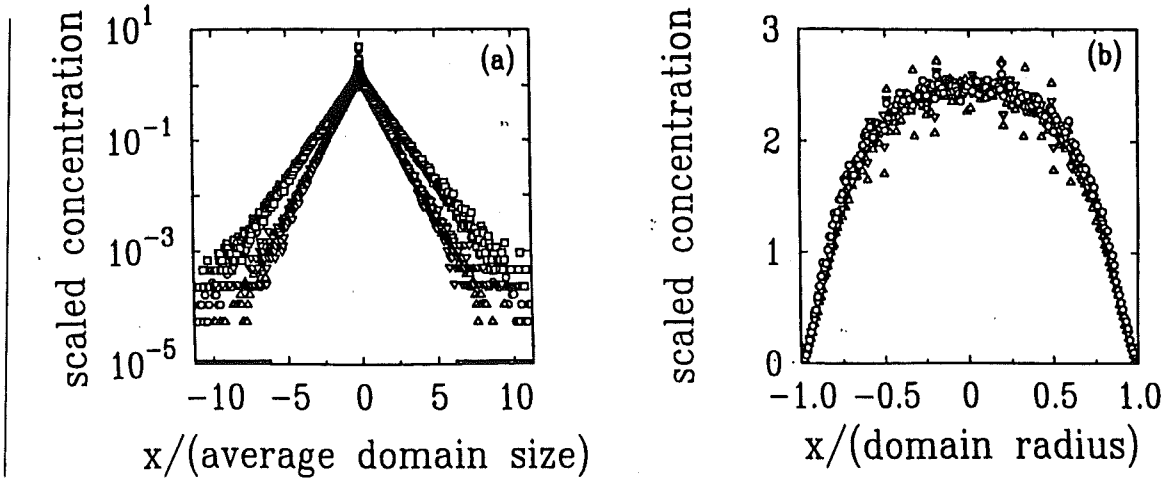

Fig. 4.3. (a) The canonical density profile of A's at $t = 194$ (o) and $t = 1477$ (□) and B's at $t = 194$ (△) and $t = 1477$ (▽) for the case of immobile B's. (b) The corresponding microcanonical density profile for the B's at $t = 194$ (△), $t = 1477$ (▽), and $t = 11222$ (o).

positive will ultimately leave a gap of the order of its length between two B particles. Thus the gaps between consecutive B's are distributed in the same way as first return times to the origin of an ordinary one-dimensional random walk [4.51], *i. e.*, as $x^{-3/2}$. From this, it follows that the domain lengths, which are the sum of the gaps of the distances between the constituent B particles, are distributed as $x^{-1/2}$.

Thus for immobile B's, the scaling form for the distribution of B domain sizes is

$$N(L,t) \sim \frac{1}{t}\Psi(L/\sqrt{t}), \tag{4.15}$$

with $\Psi(x) \sim x^{-1/2}$ as $x \to 0$ to account for the power-law tail for small domain sizes. Consequently the number of domains of fixed size L vanishes as $t^{-3/4}$ as $t \to \infty$, as has been confirmed numerically [4.37].

4.2.4 Domain Profile

A revealing physical picture of the spatial distribution of the reactants can be obtained from the average density profile of the domains. Within a scaling formulation, it is natural to define the density profile as the probability to find a particle at a fixed scaled distance from the domain midpoint, using either the typical domain size (canonical profile) or the size of the domain to which the particle actually belongs (microcanonical profile) as the rescaling factor. For the canonical profile, the ordinate is therefore proportional to the density times the number of domains. By dividing by these factors, one obtains the canonical density profile, $P^{(C)}(x)$, the probability of finding a particle at a distance $x\sqrt{Dt}$ from the center of the domain at time t. In contrast, the microcanonical profile $P^{(M)}(x)$ is obtained by superposing the density profiles of all domains, when each domain is rescaled to a fixed length, and then dividing by the product of the average concentration, the number of domains, and the average domain size.

The roughly sinusoidal microcanonical profile is reminiscent of the probability distribution for pure diffusion in a fixed size absorbing domain. In fact, the $t^{1/2}$ growth of the average domain size in two-species annihilation is at the limit of applicability of the adiabatic approximation. Thus the adiabatic approximation should provide a valid prediction for the domain profile [4.52]. For the absorbing domain $[-L(t)/2, L(t)/2]$ with $L(t)$ growing deterministically as $t^{1/2}$, the adiabatic approximation predicts the density profile $\cos(\pi x/L(t))$ (as in the case of a static absorbing domain). A more complete model is to account for the stochastic motion of the domain walls by considering the extreme particle in each of the two enclosing domains to be wall particles W, with the A's and W's reacting via $W + W \to I$ and $W + A \to W$ to describe two-species annihilation. This mapping to an exactly-soluble three-particle system of a single A between two W's [4.53] neglects the possibility that a W particle can disappear in an encounter with another W before reacting with the A. Proceeding nevertheless, we postulate that the W's diffuse with a diffusion constant D_W, so that the determination of the density profile of the A's reduces to obtaining the probability distribution of a random walker between the two absorbing wall particles. The exact solution to this three-particle problem again predicts the profile $\cos(\pi x/L(t))$, independent of the diffusion coefficients of the two species.

The linear decay of the tail of the microcanonical profile and the roughly constant concentration in the domain core provides a revealing alternative approach for determining the $t^{3/8}$ growth of the gap length ℓ_{AB} [4.54]. Within a quasi-static approximation, the density near the domain edge varies as $u/t^{3/4}$. Here u is the distance to the domain edge (defined to be at $u = 0$), and the time dependence of the denominator ensures that this density profile matches smoothly onto the core density of order $t^{-1/4}$, when $u \sim t^{1/2}$. The location of the "first" particle in this distribution, u_1, is given by the condition that there one particle in the range $[0, u_1]$, *i. e.*, $\int_0^{u_1} du'\, u'/t^{3/4} = 1$. This immediately gives $u_1 \sim t^{3/8}$, which also gives the time dependence of ℓ_{AB}.

Although the canonical and microcanonical density profiles are obtained by very different prescriptions, they are simply related. Namely, the contribution to the canonical density profile at scaled position x, is equal to the microcanonical density profile at scaled position x/α, times the probability of finding a domain of scaled length α, summed over the possible values of α. Therefore

$$P^{(C)}(x) = \int_x^\infty d\alpha\, \Phi(\alpha)\, P^{(M)}(x/\alpha), \tag{4.16}$$

where $\Phi(\alpha)$ is the scaling function for the probability of finding a domain of size $\alpha t^{1/2}$. From the large-distance asymptotic form of Φ, we immediately conclude that the large-distance tail of the canonical distribution should decay exponentially in x as is observed numerically over many decades [4.34]. An additional noteworthy feature of the canonical profile for the immobile species is the sharp peak near the origin due to the $x^{-1/2}$ singularity in the distribution of small size of B domains. In contrast, the canonical profile for the A's has a smooth peak at the origin.

It is worth mentioning that the spatial distribution of the reaction product for initially separated reactants (Sect. 4.4) appears to have the same exponential decay as the canonical profile. This feature suggests that there may be a simple explanation for the nature of the reaction zone in terms of a mapping to an equivalent single-species annihilation process.

4.2.5 Interparticle Distance Distribution

The inhomogeneity of the domain profile also governs the distribution of interparticle distances. Particles are separated by the typical interparticle separation within the core of the domain, but systematically become more sparse as the domain edge is approached. This large-scale modulation in the interparticle spacings leads to an interparticle distance distribution which is controlled both by the gap length ℓ_{AB} and the typical spacing between same species particles ℓ_{AA}.

The crucial element in the determination of the spatially averaged distance distribution is the incorporation of the density modulation within a domain. Thus to calculate the average probability of finding a local AA separation of length ℓ_{AA}, we assume a local Poisson distribution of distances, $\rho e^{-\rho \ell_{AA}}$, in which ρ is of order $t^{-1/4}$ in the domain core and vanishes *linearly* in the distance to the domain edge. Upon averaging the local Poisson distribution over this slow density variation, the spatially-averaged distribution of nearest-neighbor distances is

$$P_{AA}(x,t) \simeq x^{-2} \exp(-xt^{-1/8}), \tag{4.17}$$

where $x = \ell_{AA} t^{-1/4}$ is the scaled distance. In unscaled units, the decay length in the exponential increases as $t^{3/8}$ rather than the $t^{1/4}$ growth that would be expected naively.

From this interparticle distance distribution, the corresponding moments are,

$$\begin{aligned} M_n(t) \equiv \langle \ell_{AA}^n(t) \rangle^{1/n} &= \left[\int_0^\infty x^n \, P_{AA}(x,t)\, dx \right]^{1/n}, \\ &\sim \begin{cases} t^{1/4}, & n < 1; \\ t^{1/4} \ln t, & n = 1; \\ t^{(3n-1)/8n}, & n > 1. \end{cases} \end{aligned} \tag{4.18}$$

While numerical simulation are consistent with most of these predictions, the case $n = 1$ is somewhat problematical and the source of the discrepancy has not yet been resolved.

Rather unusual behavior occurs when one species (B) is immobile. Regions of initially closely-spaced B's contribute to the $x^{-3/2}$ tail in the probability of finding a BB closest-neighbor distance equal to x for $x < t^{1/2}$. For such a distribution, the time dependence for the reduced moments of interparticle distances between the immobile species is

$$M_n(t) \sim \begin{cases} \text{const.}, & n < 1/2; \\ \ln t, & n = 1/2; \\ t^{(2n-1)/4n}, & n > 1/2. \end{cases} \tag{4.19}$$

Due to the relatively large number of small BB distances, the reduced moments of order less than $1/2$ have a finite limiting value as $t \to \infty$, while higher-order moments grow indefinitely and are dominated by very large BB distances of the order of $t^{1/2}$. These results indicate that immobile B's have a fractal spatial distribution (see Fig. 4.0).

To generalize to higher dimensions for equally mobile species, we treat the density profile as the probability distribution of a particle diffusing within an absorbing sphere whose radius expands as $\sqrt{t}$. The adiabatic approximation still applies in this case, so that the density should decay linearly to zero in the radial coordinate near the extremity of the domain. By following exactly the same calculation as in one dimension, the reduced moments $M_n(t)$ are,

$$M_n(t) \sim \begin{cases} t^{1/4}, & n < 2; \\ t^{1/4}(\ln t)^{1/2}, & n = 2; \\ t^{(2n-1)/6n}, & n > 2. \end{cases} \tag{4.20}$$

These predictions have yet to be adequately tested, however. This stems, in part, to the algorithmic difficulty in defining a domain in higher dimensions. It is natural is to define a microcanonical density profile by superposing the profiles from one-dimensional slices through the system. This gives, however, a density which varies non-linearly in the distance to the edge of the domain. The reason for this untenable feature is as yet unresolved. It should also be noted that the limiting case of immobile B's has not been treated adequately in greater than one dimension. Indeed the B's develop a self-similar distribution (Fig. 4.0) which has not yet been properly analyzed.

4.3 Reaction with Particle Input

An important realization of two-species annihilation is the situation where reactants are continuously fed into the system. This input may arise from an constant external source [4.15-18], or from the back reaction $I \to A+B$ [4.11,55-61]. In the former case, the long-time behavior depends sensitively on the interplay between the input, the rate of transport, and the reaction itself. Although a steady state is to be anticipated when there is input, transient behavior persists if the input of the two species are not sufficiently correlated with each other. To determine the long-time behavior of the driven reaction, we make use of the fact that the equation for the concentration difference is reaction independent. This simplification permits a simple analysis of whether a steady-state is actually reached. Interestingly, the approach to the long-time asymptotic behavior for both a steadily driven reaction and a reversible system is not exponential,

as in mean-field theory, but occurs at a power law rate [4.11,55-61]. This behavior originates from the diffusive relaxation of a conserved reaction variable ($c_A - c_B$ for the steadily driven system and $c_A + c_B - 2c_I$ for the reversible system) and is therefore independent on microscopic details.

When the species are immobile, two-species annihilation with particle input is closely related to the monomer-monomer model of surface catalysis [4.19-22]. This limiting situation merits attention because of the connection with catalysis and related interacting particle models [4.40], and also because of the variety of interesting methods for analyzing this system. The input of particles now corresponds to their adsorption onto a reactive substrate whose presence promotes the transformation of neighboring A and B reactants into an AB product, which immediately desorbs from the surface. Since the input in the catalytic system is typically uncorrelated, there will be no steady state, but rather the surface eventually fills with only a single species and the reaction stops. We will discuss the rate at which this saturation phenomenon occurs.

4.3.1 Steady Input and Diffusing Reactants

For a constant feed of mobile reactants, the reaction-diffusion equations for the concentrations are

$$\frac{\partial c_{A,B}(\boldsymbol{x},t)}{\partial t} = D\nabla^2 c_{A,B}(\boldsymbol{x},t) - \mathcal{R} + \eta_{A,B}(\boldsymbol{x},t), \tag{4.21}$$

where $\mathcal{R}$ represents the reaction term whose precise form is unknown, and $\eta_{A,B}(\boldsymbol{x},t)$ are the input rates of A and B, respectively, at position $\boldsymbol{x}$ and time t. Since the reaction term is the same for both species, the concentration difference $c_-(\boldsymbol{x},t) \equiv c_A(\boldsymbol{x},t) - c_B(\boldsymbol{x},t)$ satisfies

$$\frac{\partial c_-(\boldsymbol{x},t)}{\partial t} = D\nabla^2 c_-(\boldsymbol{x},t) + \eta_-(\boldsymbol{x},t), \tag{4.22}$$

where $\eta_-(\boldsymbol{x},t) \equiv \eta_A(\boldsymbol{x},t) - \eta_B(\boldsymbol{x},t)$, and the (unknown) form of the reaction term does not enter. The solution for the instantaneous concentration difference can now be found by standard Fourier transform methods. Following ben-Avraham and Doering [4.16], it is more revealing to consider the temporally-averaged two-particle correlation function

$$\langle c_-(\boldsymbol{k},t)c_-(\boldsymbol{k}',t)\rangle = \int_0^t dt_1 \int_0^t dt_2\, e^{-Dk^2(t-t_1)-Dk'^2(t-t_2)}\langle \eta_-(\boldsymbol{k},t_1)\eta_-(\boldsymbol{k}',t_2)\rangle, \tag{4.23}$$

whose behavior depends on the precise form of the particle input.

Consider first spatially and temporally uncorrelated input with a Poisson distribution for the number of particles. Thus the noise correlation is

$$\langle \eta_A(\boldsymbol{x},t)\eta_A(\boldsymbol{x}',t')\rangle = \mathcal{N}^2 + \mathcal{N}\delta(\boldsymbol{x}-\boldsymbol{x}')\delta(t-t'). \tag{4.24}$$

Here $\mathcal{N} = \langle \eta_A(\boldsymbol{x},t)\rangle = \langle \eta_B(\boldsymbol{x},t)\rangle$ is the average number of particles injected per unit volume per unit time, and the Poissonian nature of the input is reflected

by the fact that $\langle \eta_A(\boldsymbol{x},t)^2\rangle = \mathcal{N}^2 + \mathcal{N}$. Substitution of the Fourier transform $\langle \eta_-(\boldsymbol{k},t)\eta_-(\boldsymbol{k}',t')\rangle = 2\mathcal{N}\delta(\boldsymbol{k}+\boldsymbol{k}')\delta(t-t')$ into Eq. (4.23) and inverting, gives, for the concentration difference squared at a given point in an infinite volume,

$$\langle c_-^2(\boldsymbol{x},t)\rangle = \frac{\mathcal{N}}{D}\int \frac{d\boldsymbol{k}}{(2\pi)^d}\,\frac{1-e^{-2Dk^2t}}{k^2} \sim \begin{cases} \text{const.}, & d>2 \\ \ln t, & d=2 \\ t^{(2-d)/2}, & d<2 \end{cases} \tag{4.25}$$

In a finite volume, however, the spectrum of wavenumbers is discrete. Thus at long times only a single (smallest) wavenumber dominates in the sum corresponding to the finite-volume analogue of Eq. (4.25). The long-time behavior of $\langle c_-^2(\boldsymbol{x},t)\rangle$ can therefore be estimated as the $k=0$ component of Eq. (4.25), yielding

$$\langle c_-^2(\boldsymbol{x},t)\rangle \sim t. \tag{4.26}$$

These results have a simple interpretation. In a finite volume, diffusive relaxation to spatial uniformity has time to occur and the concentration difference at a given position is governed only by imbalance in the input of A's and B's. In an infinite volume, however, diffusional relaxation modes of all time scales exist, and they aid in reducing the fluctuations compared to those characteristic of a finite volume system. Thus the growth of $\langle c_-^2(\boldsymbol{x},t)\rangle$ is slower than linear in t for $d \le 2$, while diffusive relaxation is sufficiently fast that a steady state is achieved for $d>2$.

However, a steady state is more likely to be reached for an input that explicitly conserves the particle number difference. For example, when A's and B's are introduced simultaneously (*e. g.*, from the back reaction $I \to A+B$) and at a constant rate, the noise correlation obeys $\langle \eta_-(\boldsymbol{x},t)\eta_-(\boldsymbol{x}',t')\rangle = 2\langle \eta_A(\boldsymbol{x},t)\eta_A(\boldsymbol{x}',t')\rangle - 2\langle \eta_A(\boldsymbol{x},t)\eta_B(\boldsymbol{x}',t')\rangle$, with the second term equal to $2\mathcal{N}^2 + 2\mathcal{N}\delta(t-t')p(\boldsymbol{x}-\boldsymbol{x}')$, rather than vanishing as in the case of temporally uncorrelated input. Here $p(\boldsymbol{r})$ is the probability that an AB pair is created with separation $\boldsymbol{r}$. From the Fourier transform for the noise correlation function $\langle \eta_-(\boldsymbol{k},t)\eta_-(\boldsymbol{k}',t')\rangle = 2\mathcal{N}\delta(\boldsymbol{k}+\boldsymbol{k}')[1-p(\boldsymbol{k})]\delta(t-t')$, where $p(\boldsymbol{k})$ is the Fourier transform of $p(\boldsymbol{r})$, the correlation function for $c_-(\boldsymbol{x},t)$ is

$$\langle c_-^2(\boldsymbol{x},t)\rangle = \frac{\mathcal{N}}{D}\int \frac{d\boldsymbol{k}}{(2\pi)^d}\,[1-p(\boldsymbol{k})]\,\frac{1-e^{-2Dk^2t}}{k^2}. \tag{4.27}$$

The long-time behavior of the correlation function in an infinite volume is now controlled by the small-k behavior of $p(\boldsymbol{k})$. The integral converges only if $|1-p(\boldsymbol{k})| < |\boldsymbol{k}|^\alpha$, with $\alpha > 2-d$. This, in turn, implies that $p(\boldsymbol{x}) < |\boldsymbol{x}|^{-\beta}$, with $\beta > 3-d$. Thus AB pairs must be fed in with sufficient spatial correlation to achieve steady behavior in an infinite system. For a finite-volume system, the factor $1-p(\boldsymbol{k})$ vanishes at $k=0$, which implies that steady behavior is always achieved, independent of the extent of the spatial correlation of AB pairs.

4.3.2 Approach to Asymptotic Behavior

The approach to the long-time behavior for both two-species annihilation with steady input and in the presence of back reactions follows the power law $|c_{A,B}(t) - c_\infty| \sim t^{-d/2}$ for any spatial dimension d [4.11,55-61]. This result is essentially independent of microscopic details. In contrast, the asymptotic density is approached exponentially in the mean-field limit, suggesting that the upper critical dimension of such systems is infinite. The power-law approach to the asymptotic state arises from the microscopic conservation law. The conserved quantity equals $c_A - c_B$ in the case of $A + B \to I$ with steady input, and equals $c_A + c_B - 2c_I$ for the case of $A + B \rightleftharpoons I$. Since this conserved quantity relaxes only by diffusion (although driven by the external noise in the case of $A - B$ for $A + B \to 0$ with input) an excess of the conserved quantity in a given region decays as $t^{-d/2}$.

More quantitatively, consider $P(\boldsymbol{x}, t) \equiv \langle c_-(\boldsymbol{x}, t) c_-(0,0)\rangle$. From the initial reaction-diffusion equations for the system, the equation of motion of this correlation function is

$$\frac{\partial P(\boldsymbol{x}, t)}{\partial t} = D\nabla^2 P(\boldsymbol{x}, t) \qquad \text{with} \quad P(\boldsymbol{x}, 0) = \delta(\boldsymbol{x}). \tag{4.28}$$

Such an equation holds for any linear quantity which is unaffected, on average, by the reaction (statistical conservation law). It therefore follows that $P(\boldsymbol{x}, t)$ decays as $t^{-d/2}$ in any dimension d. A similar equation holds for the case of $A + B \rightleftharpoons I$, so that identical conclusions may be drawn. A remarkable aspect of the latter result is that the system with back reactions satisfies detailed balance and tends to an uncorrelated equilibrium state, corresponding to a complete lack of interaction. Thus the existence of diffusive dynamics and a conservation law generally implies a slow approach to an equilibrium state. One can therefore conjecture a similar approach to equilibrium for the kinetic Ising model with Kawasaki dynamics, a feature which has in fact been proved by Spohn [4.62].

4.3.3 Immobile Reactants; Equivalence to Catalysis, Kinetic Ising Models, & Branching Random Walks

When the reactants are immobile, driven two-species annihilation can be regarded as an idealized catalysis model in which the input corresponds to the irreversible adsorption of gaseous reactants onto a catalytic surface, and a reaction occurs only when a nearest neighbor AB pair is created by the input [4.19-22]. These steps can be represented as,

$$\begin{aligned} A + S &\xrightarrow{k_A} A_s \\ B + S &\xrightarrow{k_B} B_s \\ A_s + B_s &\xrightarrow{k_r} (AB)\uparrow + 2S. \end{aligned} \tag{4.29}$$

If the adsorption rates for each species, k_A, k_B, are much greater than the surface reaction rate k_r, the process is *reaction-limited*, while the process is

adsorption-limited otherwise. In the adsorption-limited case, a newly-formed nearest-neighbor A_sB_s pair immediately reacts and desorbs. In the complementary reaction-limited process, an initially empty substrate quickly fills up, as any nearest-neighbor reactive pairs are quickly replaced by the (relatively) rapid input.

In the context of catalysis, the input is temporally uncorrelated, corresponding to the catalytic surface being placed in a large reservoir of reactants. The resulting non-conservation in the concentration difference implies that a finite size system is unsteady, even for equal rates of A and B input. This leads to coarsening domains of A and B, a process which ends when the surface is completely covered by only A or B and no further reaction is possible [4.22].

We will focus on the reaction-limited process because it can be solved exactly and because of its connection to disparate statistical models. (Qualitatively similar behavior occurs in the adsorption-limited case.) In an elementary reaction event, a nearest-neighbor AB pair reacts and desorbs, and the two vacated sites are immediately replenished by AA, BB, BA, or AB. When the input rates of the two species are equal, each of these possibilities occurs with probability 1/4. This system can be mapped onto a kinetic Ising model by identifying an A as a spin up, and a B as a spin down [4.38]. In the spin representation, the first two of the above pair updates correspond to single spin flip events, while the third corresponds to spin exchange. Thus the evolution of the catalytic system is equivalent to a kinetic Ising model with mixed Glauber [4.63] and Kawasaki [4.64] dynamics at $T = 0$ and $T = \infty$, respectively. The monomer-monomer catalysis model is also related to the Voter model [4.40], an interacting particle system in which each site of a lattice is in one of two states. The time evolution is defined by picking a site at random and defining its state to coincide with that of a randomly chosen nearest neighbor. This can be viewed as a population of infinitely gullible "voters" in which a randomly selected voter adopts the opinion of one of its nearest-neighbors in an elemental time increment. In spin language, this updating corresponds to a zero temperature Glauber dynamics, since spin exchange $AB \to BA$ cannot occur.

4.3.3.1 Mean-Field Theory

In the mean-field limit, the concentration of A's evolves according to

$$\dot{x} = 2(p - q)x(1 - x). \tag{4.30}$$

Here $p = k_A/(k_A + k_B)$ and $q = 1 - p$ are the relative adsorption probabilities of A and B. For $p \neq q$, the system approaches saturation exponentially quickly, with a time constant $\tau = 1/(p - q)$. When $p = q$, $\dot{x} = 0$; thus at the level of average densities the system is static.

More detailed information within the mean-field approximation is provided by the master equation for the probability distribution of the particle numbers, $P(n_A, n_B)$. To write this equation, consider the reaction on an N-site complete graph in which each pair of sites is connected. When an AB pair reacts, it is replaced by AA, BB, AB, or BA, with respectively probabilities p^2, q^2, pq, and pq, respectively. Thus $P(n_A, n_B)$ evolves according to a stochastic process

with the corresponding hopping probabilities

$$W(n_A, n_B \to n_A \pm 1, n_B \mp 1) = 2 \begin{cases} p^2 \\ q^2 \end{cases} \left(\frac{n_A}{N}\right)\left(1 - \frac{n_A}{N}\right), \tag{4.31}$$

with $W(n_A, n_B \to n_A, n_B) = 1 - W(n_A, n_B \to n_A + 1, n_B - 1) - W(n_A, n_B \to n_A - 1, n_B + 1)$. From the master equation for $P(n_A, n_B)$, the corresponding Fokker-Planck equation for $P(x)$ in the continuum limit, when $p = q$, is

$$\frac{\partial P(x,t)}{\partial t} = \frac{1}{2N}\frac{\partial^2}{\partial x^2}\left(x(1-x)P(x,t)\right). \tag{4.32}$$

The state-dependent diffusion coefficient $D(x) = x(1-x)$ reflects the probability of a reaction event being proportional to the concentration of AB pairs, $x(1-x)$. Thus the evolution of the surface concentration is analogous to diffusion in a medium that is increasingly "sticky" near the extremities of a finite absorbing interval.

The solution to the Fokker-Planck equation can be written as an eigenfunction expansion over the Gegenbauer polynomials of order 3/2 [4.22]. Interestingly, the lowest mode of this expansion is a constant, compared to the sinusoidal profile associated with diffusion on a finite absorbing interval with a spatially constant diffusion coefficient. The uniform probability distribution reflects a balance between the decrease in the diffusion coefficient near saturation and the depletion of probability at $x = \pm 1$. From the eigenfunction expansion, the survival probability $S(t) \equiv \int_0^{+1} P(x,t)\,dx$ decays exponentially at long times with a characteristic decay time equal to N; thus the typical time until a system saturates is proportional to N. The mean time until saturation for a given initial condition can be computed from the adjoint recursion formula for the first passage time to reach saturation when starting from an arbitrary initial state site [4.65]. In the continuum limit, the solution to this adjoint equation is

$$t(x) = -2N\left[(1-x)\ln(1-x) + x\ln x\right], \tag{4.33}$$

where $t(x)$ denotes the first-passage time to reach saturation, $x = 0, 1$, when the initial concentration of A's equals x. Thus the mean saturation time for system with equal initial concentration of A's and B's ($x = 1/2$) equals $2N\ln 2$, while the mean saturation time is proportional to $\ln N$ when starting very close to saturation, $x \cong 1 - 1/N$,

4.3.3.2 Mapping to a Kinetic Ising Model

Despite the inherent approximations of the mean-field approach, it provides an attractive intuitive picture of the kinetics for both the reaction-limited and adsorption-limited processes which turns out to be quantitatively valid when the substrate dimensionality d is greater than 2. However, the reaction-limited process can be solved exactly in all dimensions through the mapping onto the kinetic Ising model [4.38]. We present here the approach given by Krapivsky. The crucial aspect that leads to the solution is that the master equation for

the probability density of a spin configuration is *linear*, and the corresponding hopping rates can be written directly in terms of the spins. Due to the constraint that the square of a spin value is unity, one can decouple and thus solve the hierarchy of equations for the time dependence of spin correlations.

According to the reaction-limited monomer-monomer dynamics, the probability of a given spin configuration, $P(\{s\},t)$, evolves according to the master equation.

$$\frac{d}{dt}P(\{s\},t) = \sum_{\boldsymbol{r}}[U_{\boldsymbol{r}}(\{s\}_{\boldsymbol{r}})P(\{s\}_{\boldsymbol{r}},t) - U_{\boldsymbol{r}}(\{s\})P(\{s\},t)]+ \sum_{\boldsymbol{r},\boldsymbol{r}'}[V_{\boldsymbol{r},\boldsymbol{r}'}(\{s\}_{\boldsymbol{r},\boldsymbol{r}'})P(\{s\}_{\boldsymbol{r},\boldsymbol{r}'},t) - V_{\boldsymbol{r},\boldsymbol{r}'}(\{s\})P(\{s\},t)]. \tag{4.34}$$

Here $\{s\}_{\boldsymbol{r}}$ denotes the configuration derived from $\{s\}$ with the spin at $\boldsymbol{r}$ reversed, while $\{s\}_{\boldsymbol{r},\boldsymbol{r}'}$ has the spins at $\boldsymbol{r}$ and $\boldsymbol{r}'$ reversed. Further $U_{\boldsymbol{r}}$ is the rate at which single spin flips occur at $\boldsymbol{r}$ while $V_{\boldsymbol{r},\boldsymbol{r}'}$ is the rate at which the spin at $\boldsymbol{r}$ changes due to spin exchange between $\boldsymbol{r}$ and $\boldsymbol{r}'$, with $\boldsymbol{r}'$ a nearest-neighbor of $\boldsymbol{r}$. For the monomer-monomer catalysis model, these rates are given by

$$U_{\boldsymbol{r}}(\{s\}) = A[2z - s_{\boldsymbol{r}}\sum_{\boldsymbol{r}'} s_{\boldsymbol{r}'}] \quad V_{\boldsymbol{r}}(\{s\}) = A[1 - s_{\boldsymbol{r}}\sum_{\boldsymbol{r}'} s_{\boldsymbol{r}'}], \tag{4.35}$$

with z the lattice co-ordination number, and A an arbitrary overall rate which may be set equal to unity. Thus the first term in Eq. (4.34) gives the change in $P(\{s\},t)$ due to single spin flip events ($AB \to AA$ or $AB \to BB$), while the second term gives the contribution due to spin exchange ($AB \to BA$).

From the master equation, it can be shown that the mean magnetization at a given site $\boldsymbol{r}$ obeys the discrete Laplace equation

$$\frac{d}{dt}\langle s(\boldsymbol{r})\rangle = \Delta\langle s(\boldsymbol{r})\rangle, \tag{4.36}$$

where the discrete Laplace operator is defined as $\Delta\langle s(\boldsymbol{r})\rangle = -z\langle s(\boldsymbol{r})\rangle + \sum_{\boldsymbol{r}'}\langle s(\boldsymbol{r}')\rangle$, where $\boldsymbol{r}'$ is a nearest-neighbor of $\boldsymbol{r}$. Using standard methods, the solution for the magnetization can be expressed in terms of modified Bessel functions [4.38]. The basic feature of this solution is that the magnetization of a translationally invariant initial state remains at its initial value.

More useful information is obtained by considering the two-spin correlation function $C(x,y,t) \equiv \langle s_{ij}s_{i+x,j+y}\rangle$. In the large-distance continuum limit the correlation function obeys the diffusion equation

$$\frac{\partial C(\boldsymbol{r},t)}{\partial t} = \frac{1}{2}\nabla^2 C(\boldsymbol{r},t), \tag{4.37}$$

subject to the initial condition of $C(\boldsymbol{r},t=0) = 0$ for all non-zero $\boldsymbol{r}$, and the boundary condition $C(\boldsymbol{r}=0,t) = C(|\boldsymbol{r}| = L,t) = 1$, where L is the system length. Due to the fixed boundary condition at $\boldsymbol{r} = 0$, there will be a diffusive spread of non-zero correlation function to increasing $|\boldsymbol{r}|$. This is the underlying mechanism that leads to a coarsening pattern of A- and B-domains.

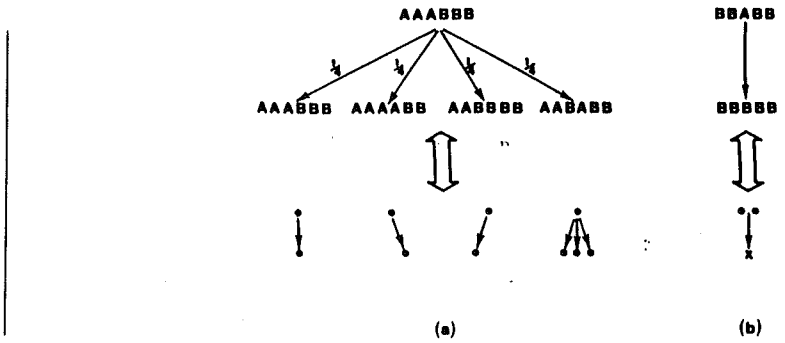

Fig. 4.4. Illustration of the mapping between the dynamics of the reaction-limited monomer-monomer catalysis model and branching annihilating random walks. (a) In a single update of the reactive AB pair, the possibilities $AB \to AB$, AA, BB, and BA, each occur with probability 1/4. These events are equivalent to the domain wall (open circle) remaining fixed, hopping to the right, hopping to the left, or branching, respectively. (b) When two domain walls meet, they annihilate.

In greater than two dimensions (mean-field limit), the correlation function approximately obeys the Laplace equation, $C(\boldsymbol{r},t) \propto 1/r^{(d-2)}$, for $r < \sqrt{t}$ and $C(\boldsymbol{r},t) \to 0$ rapidly for $r > \sqrt{t}$. Consequently, the spatial integral of the correlation function, the "correlation volume", varies as $\int^{\sqrt{t}} r^{(d-1)}\, dr \times 1/r^{(d-2)} \propto t$. When this quantity becomes of the order of the system volume, saturation occurs. Thus we conclude that the saturation time is proportional to the system volume Ω in the mean-field limit. In two dimensions and below, there is no steady solution for the correlation function for $r < \sqrt{t}$ and one must explicitly consider the full time-dependent solution. In two dimensions, this leads to the logarithmic correction, $\langle t \rangle \propto \Omega \ln \Omega$. In fact, detailed information exists about domain coarsening and spatial correlations in the closely related Voter model [4.40]. In one dimension, one finds that the spread of unit correlation function is governed by an error function profile which advances as $\sqrt{t}$. Saturation occurs when this unit correlation extends to the system length L, which leads to a saturation time which is proportional to L^2.

4.3.3.3 Mapping onto Branching Random Walks

Another creative exact solution in one dimension was developed by Takayasu and Inui in which the dynamics of domain walls (the point between two oppositely oriented sites) is mapped onto a soluble birth-death process [4.39]. In this mapping, a domain wall is a "particle" which can hop to a neighboring site, "triplicate", or annihilate with a neighboring wall upon contact in a single reaction event. These interactions can also be viewed as a mass conserving aggregation process modulo 2. Thus the mass in a finite interval is simply given by the number of domain walls in the interval (mod 2). In a single reaction event, the mass inside a fixed interval changes only by diffusion of mass into or out of the interval. Since the particles move by one lattice spacing, the mass of an interval of length r depends only on the mass within intervals of length r and $r \pm 1$ at the previous time step.

By enumerating all the ways in which the total mass within an r-interval, $M_r(t) \equiv [m_j(t) + \ldots + m_{j+r-1}(t)](\mathrm{mod}2)$ changes in a single reaction event, it is straightforward to show that the probability of finding an odd number of

particles in an interval of length r at time t obeys the recursion relation

$$P_r(t+1) = (1 - \frac{1}{N})P_r(t) + \frac{1}{2N}P_{r+1}(t) + \frac{1}{2N}P_{r-1}(t) \qquad (4.38)$$

for $r \geq 2$, where N is the number of sites in the system. (A slightly modified version of this equation holds for the special case $r = 1$) The kinetics of the catalytic system is naturally expressed in terms of the two-particle correlation function, $C_r(t) \equiv \langle \sigma_j(t)\sigma_{j+r}(t) \rangle$, where $\sigma_j(t) = 1$ if site j is occupied by an A at time t and $\sigma_j(t) = -1$ if j is occupied by a B. Then $\sigma_j(t)\sigma_{j+r}(t) = +1$ if there is an odd number of particles in the interval $[j, j+r]$ and $\sigma_j(t)\sigma_{j+r}(t) = -1$ if there is an even number of particles in $[j, j+r]$. As a consequence,

$$\langle \sigma_j(t)\sigma_{j+r}(t) \rangle = \text{prob}\{M_r(t) \text{ even}\} - \text{prob}\{\text{M}_\text{r}\text{(t) odd}\} = 1 - 2\text{p}_\text{r}\text{(t)}. \quad (4.39)$$

This linear relation between the occupation number (mod 2) inside an r-interval and the correlation function implies that these two quantities obey the same same dynamical recursion relation. In the continuum limit, this leads to the correlation function satisfying the diffusion equation, thus reproducing the results found by the Ising mapping.

4.4 Heterogeneous Reaction Conditions

Under homogeneous initial conditions, the reactants in two-species annihilation evolve into a coarsening mosaic of A- and B-domains in which the reaction rate at domain interfaces controls the kinetics. Because of the central role of these interfaces, considerable effort has recently been devoted to studying a system which is prepared with a single reactive interface, *i. e.*, initially separated components. This classic problem was apparently first studied by Zeldovich in his investigation of the combustion of unmixed gases in a virtually unknown paper [4.23]. A more recent pioneering investigation by Gálfi and Rácz [4.25] has stimulated considerable investigation [4.23-35]. This reactive configuration is also important because initially separated components are relatively simple to prepare experimentally [4.27]. The interesting geometric and dynamical features of this system provides a useful laboratory for the microscopic investigation of two-species annihilation.

There are two complementary situations under which the reaction interface may be investigated. Transient response occurs when the two components are initially separated, and then some form of mixing occurs. Due to the effective reaction-induced repulsion of opposite species, there is a weak tendency for the two components to recede from each other when diffusion is the only mode of transport. Consequently, the reaction zone, the region within which the inert product is formed, gradually increases in width, while the overall rate of reaction decreases. On the other hand, the two components may be continuously fed into the system from localized sources. For many geometries, a steady-state

is reached where reactions at the interface compensate for the input of new reactants. We will discuss the dynamical properties of the interface as a function of the geometry of the reactive system.

4.4.1 Transient response

Consider d-dimensional system which is divided in two by a $(d-1)$-dimensional hyperplane at $x = 0$. Initially A's are homogeneously distributed in the region $x > 0$ and B's are placed in the region $x < 0$. In a mean-field description, the kinetics is described by the reaction-diffusion equations

$$\frac{\partial}{\partial t} c_i(\boldsymbol{x}, t) = D_i \nabla^2 c_i(\boldsymbol{x}, t) - k c_A(\boldsymbol{x}, t) c_B(\boldsymbol{x}, t), \tag{4.40}$$

where i refers to either the A or B species, and k is the reaction constant. The appropriate initial conditions are $c_A(\boldsymbol{x}, t = 0) = c_{A0} H(x)$, and $c_B(\boldsymbol{x}, t = 0) = c_{B0} H(-x)$ where $H(x)$ is the Heaviside step function.

A straightforward dimensional analysis predicts the width of the reaction zone w and the overall reaction rate [4.25]. For simplicity, consider a one-dimensional geometry with no dependence on transverse coordinates, with $c_{A0} = c_{B0}$, $D_A = D_B$, and $k \gg 1$. Because of this latter condition, the domain of one species acts as a nearly fixed absorbing boundary condition for the opposite species. Accordingly, the density profile of the A's, for example, can be well-approximated by that associated with independently diffusing particles in the presence of a fixed absorbing boundary at $x = 0$, namely, $c_0 \operatorname{erf}(x/\sqrt{4Dt})$. The essential feature of this profile is a depletion layer of width $\sqrt{Dt}$, where the density decays linearly to zero as the absorber is approached, which matches smoothly onto the constant concentration c_0 far from the interface. The corresponding asymptotic forms of this density profile are

$$c(x,t) = \begin{cases} c_0\, x/\sqrt{4Dt} & \text{for } 0 < x \ll \sqrt{4Dt} \\ c_0 & \text{for } \sqrt{4Dt} \ll x. \end{cases} \tag{4.41}$$

The properties of the reaction interface are determined by balancing the concentration-gradient driven flux into the reaction zone, $j = -Dc' = \sqrt{\frac{D}{t}} c_0$, with the rate at which particles are annihilated. Within the mean-field approximation, the total number of reactions per unit time equals the integral of $k c_A(x,t) c_B(x,t)$ over the extent of the reaction zone. We estimate this integral as the square of a typical concentration within the zone times the zone width. The typical concentration, in turn, is of the order of $c_A(x,t)$ evaluated at $x = w$. Therefore, from Eq. (4.41), the total reaction rate is $k c(w,t)^2 w \sim k c_0^2 w^3/(Dt)$. Equating this to the flux, gives the reaction zone width as

$$w \sim (D^3 t/k^2 c_0^2)^{1/6}. \tag{4.42}$$

Correspondingly, the local production rate within the reaction zone ($\propto c(w,t)^2$) vanishes as $t^{-2/3}$.

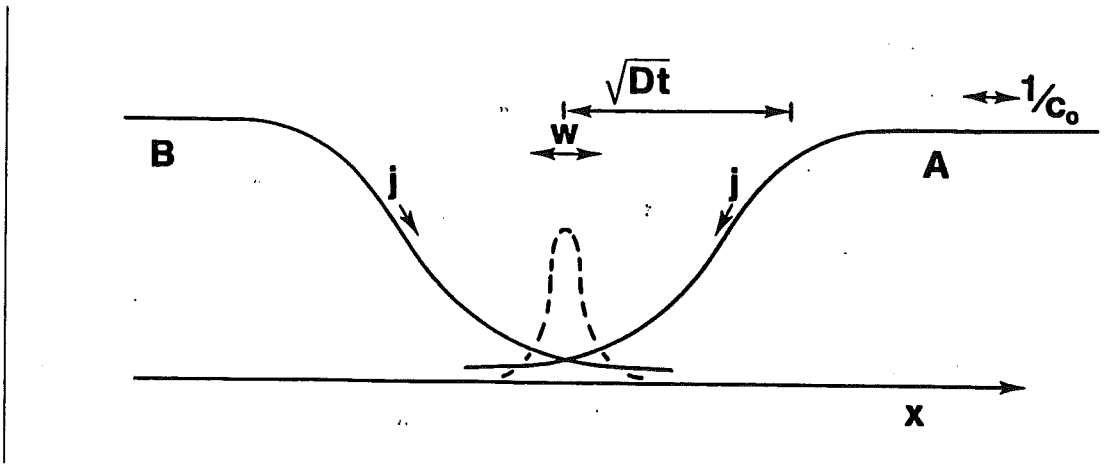

Fig. 4.5. Geometry of the reactive interface in two species-annihilation with initially separated components. For diffusive transport, there is a depletion zone of width $\sqrt{Dt}$ where the concentration decays as the opposite species domain is approached. The reaction zone is typically deep within the depletion zone.

Interestingly, w can be recast as a geometric average of basic lengths

$$w \sim (Dt)^{1/6}\, c_0^{-1/3}\, (\frac{D}{k})^{1/3} \equiv (\ell_D \ell_0 \ell_R)^{1/3}. \tag{4.43}$$

Here $\ell_D \equiv \sqrt{Dt}$ is the diffusion length, $1/c_0 \equiv \ell_0$ is the initial interparticle separation (in one dimension), and $\ell_R \equiv D/k$ is related to the "extrapolation length" associated with a semi-infinite population of reactants which obeys a radiation boundary condition at an interface [4.66]. Very roughly, this length is related to the penetration depth of A's into a partially absorbing medium whose trapping rate is related to k. This conspiracy of three independent lengths may offer a clue toward understanding the essential nature of the reaction interface.

The spatial distribution of the local production rate within mean-field theory can be obtained by employing a quasi-static approximation to Eq. (4.40). Assuming that the concentration profile is nearly linear in the reaction zone, as in Eq. (4.41), one may then write an approximation equation for the deviation of the profile from linearity by a perturbative expansion of Eq. (4.40). This resulting equation is linear and the solution can be expressed in terms of Airy functions. In the spatial region $t^{1/6} \ll x \ll t^{1/2}$, the asymptotic form of the production rate is

$$\mathcal{R}(x,t) \sim t^{-2/3} z^{3/4} \exp(-az^{3/2}), \tag{4.44}$$

where $z = x/t^{1/6}$ and a is a constant.

Numerical simulations confirm the mean-field predictions in two dimensions [4.26,29], and quantitatively similar behavior is anticipated to hold in greater than two dimensions. However the situation in one dimension is problematical. A plausible first guess is that the width of the reaction zone should be of the order of the typical distance between the nearest AB pair in the system, a distance which is expected to scale as $t^{1/4}$ [4.54]. However, simulations in one dimension indicate that $w \sim t^{\alpha}$ with $\alpha \cong 0.3$, while the local reaction rate

varies as $t^{-\beta}$ with $\beta \cong 0.8$ [4.28,30,34]. The source of this discrepancy is not yet fully resolved. Cornell and Droz have recently suggested that it is a finite-time effect and that the correct transient behavior can be inferred by analysis of the steady-state response (see the next section). Araujo *et al.* [4.35] argue that the spatial distribution of the product exhibits multiscaling in which the reduced moments $[\int dx\, x^n \mathcal{R}(x,t)]^{1/n} \sim t^{\alpha(n)}$ with $\alpha(n)$ ranging from 1/4 for $n \to 0$ to 3/8 for $n \to \infty$. Here $\mathcal{R}(x,t)$ denotes the spatial distribution of the production rate at time t. Thus they conclude that there is no unique measure of the reaction zone width, very much reminiscent of the multiscaling exhibited by the interparticle distance distribution in the homogeneous system.

When one of the species is static, the preceding mean-field approach suggest that the reaction zone width is constant, while the local production rate vanishes as $t^{-1/2}$. In one dimension, it is possible to formulate an appealing model for the stochastic recession of the boundary between the static and mobile species as reactions occur. In this approach, the static particles recede at an average rate of $1/sqrtt$ due to the flux of the mobile species, but with a superimposed random component that accounts for the discreteness of the system. By taking the simplest possible form for this fluctuating contribution and solving the resulting random walk process, one finds a reaction zone which translates at a rate of $\sqrt{t}$ and whose width grows as $t^{1/4}$. This length is a lower bound to the width of the reaction zone in the case where both species diffuse. Correspondingly, the rate production of the inert species in one dimension varies as $t^{-3/4}$.

An intriguing feature of the transient one-dimensional system is that it can exhibit short time behavior which is markedly different from that of the asymptotic limit for appropriate values of basic system parameters. For example, if the reaction rate is vanishingly small, then the two species will initially penetrate over a region whose extent grows as $\sqrt{Dt}$. Within this region, reactions will occur homogeneously, leading to an initial reaction rate which also grows as $\sqrt{Dt}$ [4.28]. However, for a low-dimensional system this penetration is eventually damped by the reaction because the effective reaction rate is infinite due to the recurrent nature of one-dimensional random walks. Another interesting phenomenon is that non-monotonic interface motion can be realized for a system with a small reaction rate when $D_A > D_B$ but $c_{A0} < c_{B0}$ [4.33]. At early times, the diffusive penetration is dominated by the faster motion of the A's and the reaction interface moves toward the B's. However, the interface motion at long times is ultimately controlled by the majority species, so that the interface moves toward the A's. This non-monotonicity has been observed on a time scale of the order of hours in a simple bimolecular reaction scheme.

4.4.2 Steady-state behavior

Complementary results for the reactive interface can be obtained for a steady system [4.32] where particles are confined to a finite d-dimensional bar with equal fluxes of A's and B's injected from opposite directions on $(d-1)$-dimensional hyperplanes. In the steady state, we can redefine the concentrations

by $c_A \Rightarrow D_B c_A$ and $c_B \Rightarrow D_A c_B$ to map the general problem to the case of equal diffusion coefficients for the two species without loss of generality. In the mean-field approximation, this system is described by the steady state version of Eq. (4.41)

$$D\nabla^2 c_A = D\nabla^2 c_B = k c_A c_B, \tag{4.45}$$

with boundary conditions $Dc'_A\big|_{x=L} = -Dc'_B\big|_{x=-L} = -j$ and $Dc'_A\big|_{x=-L} = Dc'_B\big|_{x=L} = 0$, corresponding to a constant flux of a species at one end of the system and reflection at the opposite end.

Properties of the reactive interface can be obtained by the same dimensional considerations as in the transient case. Consider first the large flux limit, which leads to a linear concentration profile near the domain boundaries, with the magnitude of the slope proportional to j/D. Since the reaction zone is the region for which the concentrations of both species are non-negligible, then the typical concentration in the reaction zone is of the order of $c_{\rm zone} \sim jw/D$. Consequently, the number of annihilation events per unit time is of order $kc_{\rm zone}^2 w$, which is obtained by integrating the reaction term over the reaction zone. Equating this number to the particle flux j then gives

$$w \sim \left(\frac{D^2}{jk}\right)^{1/3}, \tag{4.46}$$

while the typical concentration in the reaction zone is

$$c_{\rm zone} \sim jw/D \sim \left(\frac{j^2}{Dk}\right)^{1/3}. \tag{4.47}$$

These results apply as long as the width w is much less than L which corresponds, from Eq. (4.46), to $j > j_0 \sim D^2/kL^3$.

It is reassuring that the previously-derived transient behavior can be recovered by applying a quasi-static approximation to the steady-state description [4.32]. In this approach, the time derivative in the diffusion equation is neglected but the time dependence is implicitly incorporated through a moving boundary condition. For the transient system,, the growing depletion layer of order $L \sim \sqrt{Dt}$ provides the requisite moving boundary and corresponds to a time-dependent flux that is proportional to $\sqrt{Dc_0^2/t}$. Using this flux in the steady-state expression for w, Eq. (4.46), the transient result $w \sim (D^3 t/k^2 c_0^2)^{1/6}$ is recovered. *A posteriori*, the high-flux limit is appropriate, since the flux $j \sim t^{-1/2}$ is much greater than $j_0 \sim L^{-3} \sim t^{-3/2}$.

The steady behavior in both the low- and high-flux limits can be obtained by a direct analysis of the reaction-diffusion equations for $c_\pm = c_A \pm c_B$. From $c_-(x)'' = 0$, with the boundary conditions $Dc_-(x = \pm L)' = j$, one has $c_-(x) = jx/D$. Then $c_+(x)$ obeys $Dc_+(x)'' = 2kc_A c_B$, which, using $4c_A c_B = c_+^2 - c_-^2$, can be rewritten as

$$c_+(x)'' = \frac{k}{2D}\left[c_+^2 - \left(\frac{jx}{D}\right)^2\right], \tag{4.48}$$

with the boundary conditions $Dc_+(x = \pm L)' = \pm j$. Notice that this can be brought into the dimensionless form $c_+''(x) = c_+^2 - x^2$ when the length is written in units of $w_0 = (D^2/jk)^{1/3}$ and the concentration is expressed in units of $c_0 = (j^2/kD)^{1/3}$, thereby reproducing the conclusions from the large-flux dimensional analysis.

For large flux, $j > j_0$, it is easy to verify that c_+ has the power-law form,

$$c_+(z)/c_0 = (\frac{4}{5})^{1/3} + \frac{z^2}{(10)^{2/3}} - \frac{z^4}{40} + \ldots, \tag{4.49}$$

where $z \equiv x/w_0 \ll 1$. This series for c_+ matches c_- at $w \propto w_0$, thus providing an independent determination of the reaction zone width.

Outside the reaction zone, the concentration of the minority species can be obtained directly by substituting the large-x approximation $c_A \cong c_B + (jx/D)$ in the steady-state equation for c_B to give $Dc_B(x)'' = kc_B(c_B + jx/D)$. This reduces to the Airy equation $c_B(z)'' = z\, c_B(z)$ for $z \gg 1$ with solution is

$$c_B(x)/c_0 \sim z^{-1/4} \exp\big(-2z^{3/2}/3\big). \tag{4.50}$$

Thus in the high flux limit, the concentration of B's is approximately $-jx/D$ for $x < -w$, exponentially small for $x > w$, and equal to $(c_+ - c_-)/2 \propto j^{2/3}$ in the reaction zone. The concentration of A's is the mirror image of $c_B(x)$ about $x = 0$.

In the low flux limit, the density varies weakly in space, and it can be easily verified that

$$c_+(x) \cong \sqrt{\frac{2j}{kL}} + \left(\frac{j}{2DL}\right) x^2 \tag{4.51}$$

is an accurate approximation for the entire domain $[-L, L]$. The second term is determined by the boundary conditions on c_+ at $x = \pm L$, and the leading term is then determined from Eq. (4.48). Notice that the magnitude of the concentration variation ($\sim j$) is small compared to the value of the concentration itself ($\sqrt{j}$). An interesting feature which emerges results is that the local reaction rate $\mathcal{R}(x) \equiv kc_A(x)c_B(x)$ is unimodal for large flux and bimodal otherwise. That is, for $j > j_0$, $\mathcal{R}(x) \propto (jw)^2 - \text{const.} \times (jx)^2$, so that the reaction rate is large only within a region of width w_0 about $x = 0$, while for $j < j_0$, $\mathcal{R}(x) \propto j + \text{const.} \times j^{3/2}x^2$, so that the reaction rate is large only near the edges of the system.

The validity of the mean-field approximation and the nature of the steady state in a one-dimensional system has been investigated only very recently, and the results may also shed light on the puzzling behavior of the corresponding transient system [4.34]. On dimensional grounds, the system is characterized by three basic parameters, namely j, D and k. In spatial dimension $d \leq 2$, the recurrence of random walks implies that particles meet infinitely often, and hence react, irrespective of k. Thus the reaction rate can be disregarded. It then follows that the only length in the system is $(D/j)^{1/(d+1)}$. In one dimension, this gives an interface width which scales as $j^{-1/2}$. Furthermore, the mean-field

result of $w \propto j^{-1/3}$ is recovered for $d = 2$, indicating that $d = 2$ is indeed the upper critical dimension for this problem.

This line of reasoning relies crucially on the time independence of the reaction, so that the width of the reaction zone is fixed by the unique dimensional length scale. In contrast, several independent lengths exist for the transient system, and the interface width cannot be obtained unambiguously through dimensional analysis alone. However, one can infer the transient behavior by again applying the quasi-static approximation to the steady state results. As discussed above, the flux in the transient system decreases as $t^{-1/2}$ which, when substituted into $w \propto j^{-1/2}$ gives $w \propto t^{1/4}$ [4.34].

Another remarkable property of the one-dimensional system is the large-distance behavior of the reaction profile. Whereas mean-field theory predicts an $\exp(-x^{3/2})$ decay of the density of the reaction product at large distances, it is found numerically that the decay is a pure exponential [4.30]. The exponential decay is particularly puzzling in light of the fact that in the large-distance asymptotic region there is a well-defined majority species with little fluctuations. Under these circumstances, the mean-field prediction is expected to hold in this region (S. Cornell, private communication).

The above approaches can be extended in several interesting ways [4.32]. One physically-relevant situation is when reactants drift toward each other, as would occur if two oppositely charged species were in a uniform electric field. For relatively weak drift, the density profile of each species is nearly constant and of order j/v outside a boundary layer of thickness D/v, and varies linearly with position inside the boundary layer where diffusion predominates. This reasoning is valid as long as the thickness of the boundary layer D/v is larger than the reaction zone width $(D^2/jk)^{1/3}$, or, equivalently, $v < v_0 \sim (Djk)^{1/3}$.

Another example is an annular geometry in which a flux j of B's is injected at an inner radius r_1, and a flux $-j$ of A's is injected at outer radius r_2. When both radii are large with their difference remaining finite, the solution to the radial Laplace equation for the concentration difference predicts that the reaction zone center is at $r_0 \cong (r_1 + r_2)/2$, with the density profiles and the reaction zone width behaving in the same manner as in one dimension. However, if $r_2/r_1 \to \infty$, then the reaction zone center remains very close to the inner radius with $r_0 \cong r_2/\sqrt{e}$ for $d = 2$ and $r_0 \cong 2r_2/3$ for $d = 3$ [4.32]. When one species is injected at a point in a background medium of the opposite species rather different behavior occurs. When both species are mobile, the reaction zone center is at $r_0 \sim \sqrt{t \ln t}$ and the width of the zone is proportional to $t^{1/6}$ times a logarithmic correction, within mean-field theory [4.67]. When the background consists of immobile particles, then the number of injected particles which remain unreacted increases slower than linear in time for $d = 3$ [4.68]. These radial geometries offer a new range of phenomena that merit further exploration.

4.5 Concluding Remarks

In diffusion-limited two-species annihilation, an initially homogeneous distribution of A's and B's at equal initial densities evolves into a mosaic of growing single species domains. When both species are equally mobile, the concentration within the domain core is roughly uniform and proportional to $t^{-d/4}$, while the concentration vanishes linearly in the distance to the domain edge for spatial dimension $d \leq 2$. This linear decay leads to a new length scale, ℓ_{AB}, intermediate to the typical interparticle spacing and the typical domain size, as well as multiscaling in the reduced moments $\langle \ell_{AA}^n(t) \rangle^{1/n}$. When one species is immobile, the domains of immobile species evolve only by infiltration of mobile species from the exterior, and vestiges of the initial distribution persist in the domain interior. This leads to a power law distribution for the separations of the immobile particles in which, $\langle \ell_{BB}^n(t) \rangle^{1/n}$ appears to increase as a power law in time for $n \geq 1/2$, but approaches a finite limiting value for $n < 1/2$.

In higher dimensions, there is less understanding of domain structure and the spatial organization of reactants. A good algorithm is needed to unambiguously define domains in greater than one dimension. This would aid in addressing questions such as the distribution of domain sizes, the nature of the density profile within a domain, and the spatial organization of the domains. Numerical evidence indicates that anomalous scaling of interparticle distances exists in $d = 2$ but not in $d = 3$. Thus $d = 3$ appears to be a critical dimension above which there is no substantial depletion layer at the periphery of a domain.

There are several generalizations of two-species annihilation that raise a variety of interesting questions. For example, consider immobile reactants in which the reaction is mediated only by long-range exchange [4.69,70]. For an exchange rate which decreases exponentially in the particle separation, the density decays as $(\ln t/\tau)^{-d/2}$ and large-scale reactant segregation ensues. Another potentially important situation is two-species annihilation in the presence of (unscreened) Coulomb forces. A scaling argument suggests that the decay is mean-field-like in all dimensions [4.71], but this has yet to be tested numerically. Anomalous initial conditions, such as a lamellar configuration, are also found to influence the kinetics [4.72,73]. Many of the interesting properties of two-species annihilation also arise in related stoichiometries such as higher-order reactions [4.74] and n-species reactions [4.75]. In particular, in two-species competition [4.76-78] species A and B evolve both by logistic growth (with the associated rate equation $\dot{c} = k_1 c - k_2 c^2$) and mutual annihilation. This can be regarded as a prototypical model for interspecies competition in a biological context. A homogeneous initial state evolves into single-species domains which coarsen logarithmically in one dimension and at a power law rate in two dimensions. This latter growth strongly resembles that observed in spinodal decomposition [4.79].

With constant input of reactants, there is a relatively good understanding of the conditions needed to achieve a steady state. Typically, a steady state

is reached when there is complete temporal correlation and relatively strong spatial correlation of particle-antiparticle pairs. The situation where the reactants are immobile is particularly noteworthy because of the connection to the monomer-monomer catalysis model. This model is exactly soluble in all dimensions by a mapping onto a kinetic Ising model. Close connections also exist with the voter model and with branching random walks. All of these connections provide useful insights for understanding the basic mechanism of domain coarsening and saturation in the monomer-monomer model.

At the microscopic level, two-species annihilation is controlled by the rate at which reactions occur at the interface between A and B domains. This observation, together with recent experimental work, provides the motivation for considering geometries which possess a single reaction interface. From analysis of the reaction-diffusion equations or by dimensional analysis, geometrical properties and the reactivity of the reaction zone at an AB interface can be determined. The one-dimensional case is especially intriguing as there are indications that many length scales are needed to characterize the reaction zone. This focus on the reaction interface in microscopic modelling may prove fruitful for other reactions. A classic example is that of the growth and wave-like spread of a localized population whose dynamics is governed by logistic growth [4.74,80,81]. While mean-field theory predicts the existence of a soliton-like propagating wave front, an exact solution in one dimension shows that the width grows as $\sqrt{t}$ [4.82], while numerical simulations [4.83] indicate that the width grows in same manner as that KPZ-like growth [4.84].

Acknowledgements.

We thank D. ben-Avraham, E. Ben-Naim, D. Considine, K. Kang, P. Meakin, G. Murthy, H. Takayasu, and J. Zhuo for pleasant collaborations on various aspects of reaction kinetics. We have also greatly benefitted from helpful discussions with M. Araujo, E. Clément S. Cornell, M. Droz, S. Havlin, H. Larralde, and G. Zumofen. We also thank E. Ben-Naim, S. Havlin, and H. Larralde for a critical reading of the manuscript and helpful suggestions. Finally, we gratefully acknowledge grants DAAL03-86-K-0025 and DAAL03-89-K-0025 from the ARO, INT-8815438 from the NSF, DGAPA project IN100491, and project #903922 from CONACYT for partial financial support of this research.

References

4.1 For recent reviews on two species annihilation see *e. g.*, Ya. B. Zeldovich, A. S. Mikhailov: Sov. Phys. – Usp. **30**, 23 (1988);
V. Kuzovkov, E. Kotomin: Rep. Prog. Phys. **51**, 1479 (1988);
R. Kopelman: Science **241**, 1620 (1988);
A. S. Mikhailov: Phys. Repts. **184**, 307 (1989);
A. A. Ovchinnikov, S. F. Timashev, A. A. Belyy: *Kinetics of Diffusion Controlled Chemical Processes* (Nova Science Publishers, 1990)

4.2 Z. Vardeny, P. O'Connor, S. Ray, J. Tauc: Phys. Rev. Lett. **44**, 1267 (1980)

4.3 I. M. Campbell: *Catalysis at Surfaces* (Chapman and Hall, New York, 1988); G. C. Bond: *Heterogeneous Catalysis: Principles and Applications* (Clarendon Press, Oxford, 1987)
4.4 W. M. Yen, P. M. Selzer, eds.: *Laser Spectroscopy of Solids, 2nd ed.* (Springer-Verlag, Berlin, 1986)
4.5 J. Preskill: Phys. Rev. Lett. **43**, 1365 (1979)
4.6 M. Bramson, J. L. Lebowitz: Phys. Rev. Lett. **61**, 2397 (1988); M. Bramson, J. L. Lebowitz: J. Stat. Phys. **62**, 297 (1991); M. Bramson, J. L. Lebowitz: J. Stat. Phys. **65**, 941 (1991)
4.7 Ya. B. Zeldovich, A. A. Ovchinnikov: Chem. Phys. **28**, 215 (1978)
4.8 S. F. Burlatskii: Sov. Theor. Exp. Chem. **14**, 483 (1978)
4.9 S. F. Burlatskii, A. A. Ovchinnikov: Russ. J. Phys. Chem. **52**, 1635 (1978)
4.10 D. Toussaint, F. Wilczek: J. Chem. Phys. **78**, 2642 (1983)
4.11 K. Kang, S. Redner: Phys. Rev. Lett. **52**, 955 (1984); Phys. Rev. A **32**, 435 (1985)
4.12 K. Lee, E. J. Weinberg: Nucl. Phys. B **246**, 354 (1984)
4.13 P. Meakin, H. E. Stanley: J. Phys. A **17**, L173 (1984)
4.14 G. Zumofen, A. Blumen, J. Klafter: J. Chem. Phys. **82**, 3198 (1985)
4.15 L. W. Anacker, R. Kopelman: Phys. Rev. Lett. **58**, 289 (1987); L. W. Anacker, R. Kopelman: J. Chem. Phys. **91**, 5555 (1987)
4.16 D. ben-Avraham, C. R. Doering: Phys. Rev. A **37**, 5007 (1988)
4.17 K. Lindenberg, B. J. West, R. Kopelman: Phys. Rev. Lett. **60**, 1777 (1988)
4.18 E. Clément, L. M. Sander, R. Kopelman: Phys. Rev. A **39**, 6455 (1989); Phys. Rev. A **39**, 6466 (1989)
4.19 R. M. Ziff, K. Fichthorn: Phys. Rev. B **34**, 2038 (1986)
4.20 P. Meakin, D. Scalapino: J. Chem. Phys. **87**, 731 (1987)
4.21 K. Fichthorn, E. Gulari, R. M. Ziff: Phys. Rev. Lett. **63**, 1527 (1989)
4.22 D. ben-Avraham, D. Considine, P. Meakin, S. Redner, H. Takayasu: J. Phys. A **23**, 4297 (1990); D. ben-Avraham, S. Redner, D. Considine, P. Meakin: J. Phys. A **23**, L613 (1990)
4.23 Ya. B. Zeldovich: Zh. Tekh. Fiz. **19**, 1199 (1949)
A. S. Mikhailov: in [4.1]
4.24 I. M. Sokolov: Sov. Phys. JETP Letters **44**, 67 (1986)
4.25 L. Gálfi, Z. Rácz: Phys. Rev. A **38**, 3151 (1988)
4.26 Z. Jiang, C. Ebner: Phys. Rev. A **42**, 7483 (1990)
4.27 Y.-E. L. Koo, L. Li, R. Kopleman: Mol. Cryst. Liq. Cryst. **183**, 187 (1990); Y.-E. L. Koo, R. Kopleman: J. Stat. Phys. **65**, 893 (1991)
4.28 H. Taitelbaum, S. Havlin, J. E. Kiefer, B. Trus, G. H. Weiss: J. Stat. Phys. **65**, 873 (1991)
4.29 S. Cornell, M. Droz, B. Chopard: Phys. Rev. A **44**, 4826 (1991)
4.30 M. Araujo, S. Havlin, H. Larralde, H. E. Stanley: Phys. Rev. Lett. **68**, 1791 (1992); H. Larralde, M. Araujo, S. Havlin, H. E. Stanley: Phys. Rev. A **46**, 855 (1992)
4.31 H. Larralde, M. Araujo, S. Havlin, H. E. Stanley: Phys. Rev. A **46**, 6121 (1992)
4.32 E. Ben-Naim, S. Redner: J. Phys. A **25**, L575 (1992)
4.33 H. Taitelbaum, Y.-E. L. Koo, S. Havlin, R. Kopelman, G. H. Weiss: Phys. Rev. A **46**, 2151 (1992)
4.34 S. Cornell, M. Droz: Phys. Rev. Lett. **xx**, xx (1993)
4.35 M. Araujo, H. Larralde, S. Havlin, H. E. Stanley: preprint
4.36 The importance of of interparticle distributions in two-species annihilation was apparently first raised in P. Argyrakis, R. Kopelman: Phys. Rev. A **41**, 2121 (1990)
4.37 F. Leyvraz, S. Redner: Phys. Rev. Lett. **66**, 2168 (1991); Phys. Rev. A **46**, 3132 (1992)
4.38 E. Clément, P. Leroux-Hugon, L. M. Sander: Phys. Rev. Lett. **67**, 1661 (1991)
P. L. Krapivsky: Phys. Rev. A **45**, 1067 (1992); J. Phys. A **25**, 5831 (1992)
4.39 H. Takayasu, N. Inui: J. Phys. A **25**, L585 (1992)
4.40 T. J. Cox, D. Griffeath: Ann. Probab. **14**, 347 (1986);
For general results about the voter model, see *e. g.*, R. Durrett: *Lecture Notes on Particle Systems and Percolation* (Wadsworth & Brooks/Cole, Pacific Grove, CA, 1988)
M. Scheucher, H. Spohn: J. Stat. Phys. **53**, 279 (1988)
4.41 K. Lindenberg, B. J. West, R. Kopelman: Phys. Rev. A **42**, 890 (1990)
4.42 S. Cornell, M. Droz, B. Chopard: Physica A **188**, 322 (1992)
4.43 See *e. g.*, S. Havlin, D. ben-Avraham: Adv. Phys. **36**, 695 (1987)

4.44 W.-S. Sheu, K. Lindenberg, R. Kopelman: Phys. Rev. A **42**, 2279 (1990); K. Lindenberg, W.-S. Sheu, R. Kopelman: Phys. Rev. A **43**, 7070 (1991); K. Lindenberg, W.-S. Sheu, R. Kopelman: J. Stat. Phys. **65**, 1285 (1991);
4.45 G. Zumofen, J. Klafter, A. Blumen: Phys. Rev. A **43**, 7068 (1991); G. Zumofen, J. Klafter, A. Blumen: J. Stat. Phys. **65**, 1015 (1991)
4.46 F. Leyvraz: J. Phys. A **25**, 3205 (1992)
4.47 M. Bramson, D. Griffeath: Z. Wahrsch. verw. Gebiete **53**, 183 (1980)
4.48 D. C. Torney, H. M. McConnell: Proc. Roy. Soc. London Ser. A **387**, 147 (1983); A. A. Lushnikov: Sov. Phys. JETP **64**, 811 (1986)
4.49 J. L. Spouge: Phys. Rev. Lett. **60**, 873 (1988)
4.50 C. R. Doering, D. ben-Avraham: Phys. Rev. A **38**, 3035 (1988); D. ben-Avraham, M. A. Burschka, C. R. Doering: J. Stat. Phys. **60**, 695 (1990)
4.51 See *e. g.*, W. Feller: *An Introduction to Probability Theory and its Applications* (Wiley, New York, 1968), Vol. 1
4.52 See *e. g.*, L. D. Landau, E. M. Lifshitz: *Quantum Mechanics* (Pergamon Press, New York, 1977).
4.53 F. Leyvraz: unpublished notes; D. ben-Avraham: J. Chem. Phys. **88**, 941 (1988) M. E. Fisher, M. P. Gelfand: J. Stat. Phys. **53**, 175 (1988)
4.54 This approach for finding the "last" particle in a distribution was first considered for the case of a fixed by trap by G. H. Weiss, S. Havlin, R. Kopelman: Phys. Rev. A **39**, 466 (1989); S. Redner, D. ben-Avraham: J. Phys. A **23**, L1169 (1990); S. Havlin, H. Larralde, R. Kopelman, G. H. Weiss: Physica A **169**, 337 (1990)
4.55 Ya. B. Zel'dovich, A. A. Ovchinnikov: Sov. Phys. JETP Letters **26**, 440 (1977)
4.56 Ya. B. Zeldovich, A. A. Ovchinnikov: Sov. Phys. JETP **47**, 829 (1978)
4.57 S. F. Burlatskii, A. A. Ovchinnikov: Sov. Phys. JETP **65**, 908 (1987)
4.58 Y.-C. Zhang: Phys. Rev. Lett. **59**, 1726 (1987)
4.59 S. F. Burlatskii, A. A. Ovchinnikov, G. S. Oshanin: Sov. Phys. JETP **68**, 1153 (1989)
4.60 N. Agmon, A. Szabo: J. Chem. Phys. **92**, 570 (1990)
4.61 D. Huppert, S. Y. Goldberg, A. Masad, N. Agmon: Phys. Rev. Lett. **68**, 3932 (1992)
4.62 H. Spohn, in: *Statistical Physics and Dynamical Systems: Rigorous Results*, eds. L. Fritz, A. Jaffe, D. Szász, (Birkhäuser, 1985)
4.63 R. J. Glauber: J. Math. Phys. **4**, 294 (1963)
4.64 K. Kawasaki, in: *Phase Transitions and Critical Phenomena*, eds. C. Domb and M. S. Green (Academic, New York, 1976) 4.64 kawasaki model
4.65 G. H. Weiss: Adv. Chem. Phys. **13**, 1 (1966); J. Stat. Phys. **24**, 587 (1981)
4.66 E. Ben-Naim, S. Redner, G. H. Weiss: J. Stat. Phys. **xx**, xx (1993)
4.67 E. Ben-Naim, S. Redner: unpublished
4.68 H. Larralde, Y. Lereah, P. Trunfio, J. Dror, S. Havlin, R. Rosenbaum, H. E. Stanley: Phys. Rev. Lett. **xx**, xxx (1993).
4.69 J. R. Eggert: Phys. Rev. B **29**, 6664 (1984); T. M. Searle, J. E. L. Bishop: Philos. Mag. B **53**, L9 (1986)
4.70 H. Schnörer, V. Kuzovkov, A. Blumen: Phys. Rev. Lett. **63**, 805 (1989)
4.71 T. Ohtsuki: Phys. Lett. A **106**, 224 (1984)
4.72 F. J. Muzzio, J.M. Ottino Phys. Rev. Lett. **63**, 47 (1989); Phys. Rev. A **42**, 5873 (1990)
4.73 I. M. Sokolov, A. Blumen: Phys. Rev. A **43**, 2714 (1991)
4.74 K. Kang, P. Meakin, J. H. Oh, S. Redner: J. Phys. A **17**, L665 (1984)
4.75 D. ben-Avraham, S. Redner: Phys. Rev. A **34**, 501 (1986)
4.76 J. D. Murray, *Mathematical Biology*, (Springer-Verlag, Berlin, 1989)
4.77 S. F. Burlatskii, K. A. Pronin: J. Phys. A **22**, 531 (1989)
4.78 J. Zhuo, G. Murthy, S. Redner: J. Phys. A **25**, 5889 (1992)
4.79 See: *e. g.*, J. D. Gunton, M. San Miguel, P. S. Sahni: in *Phase Transitions and Critical Phenomena*, Vol. 8, C. Domb, J. L. Lebowitz, Editors (Academic Press, London, 1984);
4.80 A. Kolmogorov, I. Petrovsky, N. Piscounov: Moscow Univ. Bull. Math. **1**, 1 (1937)
4.81 R. A. Fisher: Ann. Eugenics **7**, 353 (1937)
4.82 C. R. Doering, M. A. Burschka, W. Horsthemke: J. Stat. Phys. **65**, 953 (1991)
4.83 E. Ben-Naim, S. Redner: unpublished
4.84 M. Kardar, G. Parisi, Y.-C. Zhang: Phys. Rev. Lett. **56**, 889 (1986)

This article was processed by the author using the TEX Macropackage from Springer-Verlag.